

Supplemental Material

Methods: Description of Animal Model Studies

University of Utah Institutional Animal Care and Use Committee approval was obtained for all animal experimentation. Five juvenile swine weighing 30 to 35 kgs were sedated with a cocktail of Telazol 4.4 mg/kg, Ketamine 2.2 mg/Kg and Xylazine 2.2 mg/Kg intra-muscularly and were placed on mechanical ventilation. Anesthesia was maintained with intravenous injections of 30-40 mg/Kg of pentobarbital. The femoral veins and arteries were accessed via cut down technique. 11 Fr. sheaths (St. Jude Medical, Austin, TX) were placed in the right and left femoral vein and were used to insert a mapping and ablation catheter. A 6 Fr. sheath was placed in the right femoral artery and was used for blood pressure monitoring and obtaining periodic arterial samples for blood gas analysis.

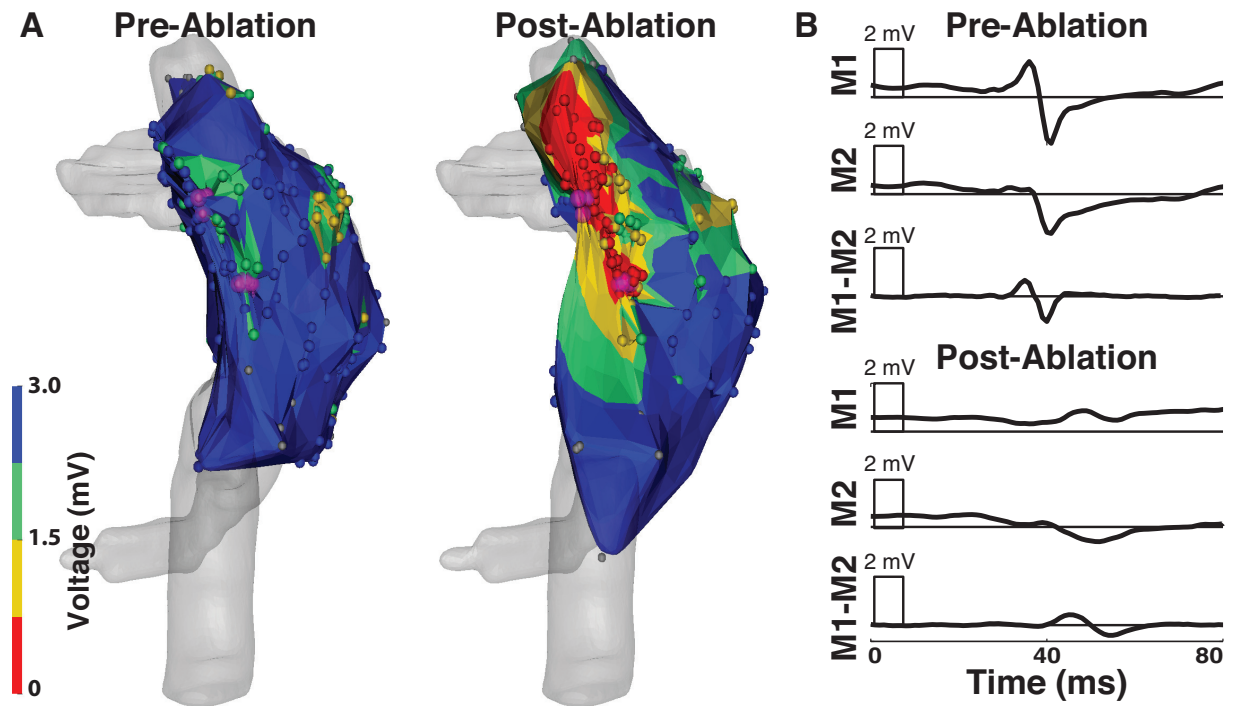


Figure 1: In vivo model of electroanatomical substrate mapping. A. Voltage maps acquired in a porcine right atrium pre- and postablation displaying bipolar amplitude. The purple spheres represent ablation points, all other points represent measurement sites colored according to bipolar amplitude. B. Representative electrograms acquired from the same location in the right atrium pre- and postablation. EAM - electroanatomical map, M1 and M2 - unipolar electrograms from the distal and proximal electrodes of a mapping catheter, M1-M2 - bipolar electrogram.

Anesthetized animals were moved to the electrophysiology lab with fluoroscopy (Artis Zeego, Siemens USA, Malvern, PA) and a CARTO XP electroanatomical mapping system (Biosense Webster, Diamond Bar, CA). A non-irrigated 4 mm tip NaviStar (Biosense Webster, Diamond

Bar, CA) catheter was used for electro-anatomical mapping. Baseline voltage maps were acquired and followed by the creation of two ablation lesions approximately 1 cm apart by delivering RF energy at 30 W for 30 seconds each in a temperature-controlled mode (60°C cutoff). During ablation we acquired mapping points every 5 to 10 seconds to ensure the catheter did not move. The center of each successfully ablated regions in the electroanatomical maps was estimated by calculating the centroid of all points acquired during the ablation. Immediately following the final ablation, the entire RA was remapped with particular emphasis on the areas surrounding the ablation sites with 142 ± 59 (min = 72, max = 194) points acquired per map (Figure 1A). The bipolar amplitude, Δ LAT, and Euclidean distance from the nearest ablation lesion center were calculated for each mapping point. Following the ablation and mapping studies, we intravenously injected each swine with 2,3,5-Triphenyl-2H-tetrazolium chloride (2% TTC), which demarcates ablated and infarcted tissues by staining live tissue red^{1,2}. This step was immediately followed by lethal injection of intravenous potassium chloride.

Methods: Estimating the Extent of Ablation Injury

Ablation of cardiac tissue is known to cause immediate changes to the electrophysiological properties of directly targeted regions as well as surrounding tissues. These changes include cell death through membrane rupture, protein denaturing, stunning, and edema, all of which are known to affect BPAs to some degree³⁻⁶. Due to these factors it is challenging to appropriately demarcate which low voltages are due to actual injury (true positives), and those that arise because of factors unrelated to the health of the myocardial substrate (false positives). Consequently, we evaluated the extent of ablation injury, first, by gross pathological examination of the lesion sets, and, second, by analysis of postablation BPAs surrounding the lesion sites. The gross pathological analysis provided a stringent bound of ablation impact within which low voltage BPAs were strongly expected. We selected the loose bound based on analysis of the spatial transition of BPAs from low to normal voltages as distance from the lesion increased. These two bounds (described in more detail below) characterize the range of sensitivities and specificities that might be achieved with voltage mapping.

Gross Pathology of Ablation Lesions Lesion formation was confirmed by gross pathological assessment of the RA tissue. Lesion size was recorded based on two orthogonal measurements of the edge to edge diameter. Specifically, we acquired photographs of each lesion set, including a reference metric ruler, with a digital camera (Canon, Tokyo, Japan). The image analysis software GraphicConverter X v7.6.1 (Lemkesoft GmbH, Peine, Germany) was used to convert pixel size to millimeters via the reference ruler and then measure the lesion diameter with digital calipers using the boundary of the TTC staining. If the lesion shape was eccentric, its two principal axes were measured, otherwise axis orientation was arbitrary.

Kernel Regression Analysis Low voltage BPAs in the postablation maps were observed frequently beyond the anticipated burn radius (\approx 3-4 mm, Figure 2). We assumed that these low voltages were associated with the acute but transient injury responses to ablation. To estimate the outer range of low voltage BPAs, we used an approach known as kernel regression which is a non-parametric technique for estimating the conditional expectation of a random variable^{7,8}. Software implementations of this technique are available in the open source statistical analysis package, R (The R Project for Statistical Computing, <http://www.r-project.org>). We used kernel

regression to analyze the relationship between BPAs (pre- and postablation) and the site of EGM acquisition relative to the lesion center. The mean BPA and ± 3 standard deviations were calculated for the pre- and postablation maps and the distance at which the respective error bars crossed was assigned as the loose boundary for expected low voltages (Figure 2).

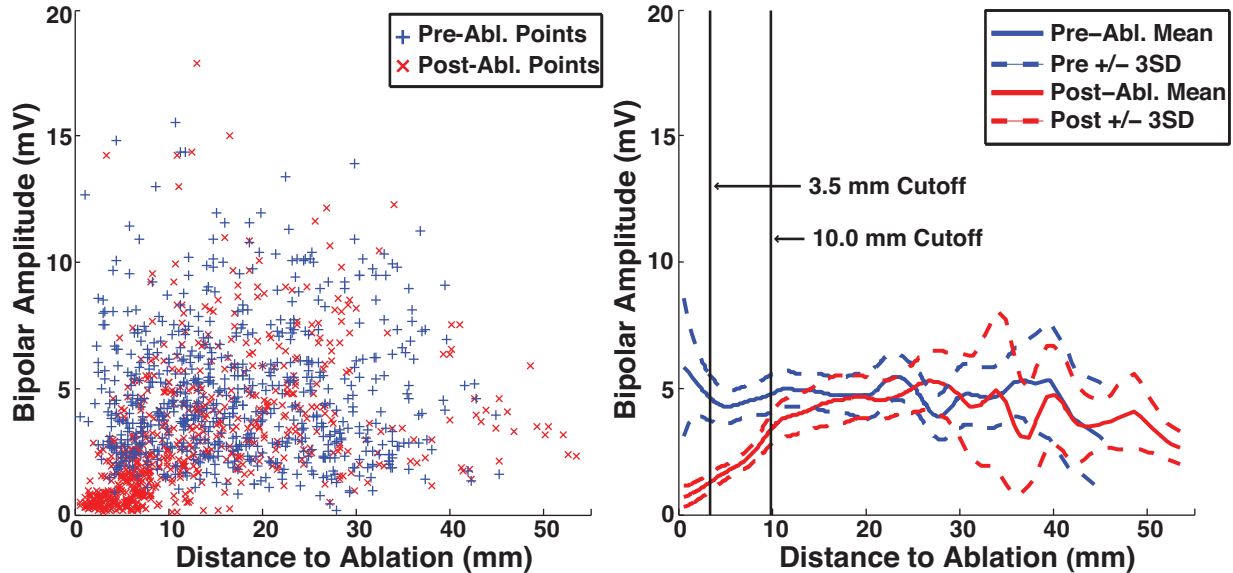


Figure 2: Evolution of BPA with respect to distance from ablation site. Left – Postablation points (red) and preablation points (blue) are plotted based on their BPA and distance from the centroid of the nearest ablation site. Right – Mean and error bars (3 standard deviations) of the pre- (blue) and postablation (red) voltage maps as a function of distance from ablation sites based on kernel regression analysis. The 3.5 mm cutoff represents the mean radius of lesions as measured by gross pathology. The 10.0 mm cutoff is the point at which the pre- and post ablation error bars cross in the kernel regression analysis.

Results: Animal Model

We performed electroanatomical mapping, ablation, and gross pathological analysis in all animals. There were no low voltage regions, i.e., areas with multiple, closely spaced low voltage recordings, in the preablation mapping of the swine right atria. The mean preablation bipolar amplitude was 4.74 ± 2.62 mV ($n = 666$). Following ablation, low voltage BPAs were observed in proximity to all attempted ablation sites (for an example, see Figure 1B). The mean diameter of all lesions was 7.3 ± 1.6 mm ($n = 20$ measures of 10 lesions, max = 10.1 mm, min = 4.5 mm). The lesions were mostly circular in shape with only one lesion presenting an anisotropy ratio greater than 2:1. Reasoning that tissue directly targeted by ablation would have the greatest likelihood of displaying low BPAs we estimated these regions based on the mean radius of the lesions from the gross pathological analysis and chose 3.5 mm from the lesion center as the stringent boundary. BPAs acquired within the stringent bound showed significantly lower voltages, 0.84 ± 1.64 mV ($n = 78$), than EGMs acquired outside the 3.5 mm stringent bound (3.38 ± 2.58 mV, $n = 632$). Figure 2 illustrates the spatial transition of post-ablation BPAs from low voltage at points near ablation centers to normal voltage at points remote from ablation. The

error bars (± 3 standard deviation) of the pre- and postablation kernel regression plots intersected at 10 mm from the lesion center. We selected this distance as the loose bound for the expectation of low voltages surrounding an ablation lesion. BPAs within the loose bound (10.0 mm from the lesion center) had significantly lower voltages (1.78 ± 1.71 mV, $n = 351$), than bipolar EGMs acquired outside the 10 mm threshold (4.39 ± 2.71 mV, $n = 359$).

References

1. Kim RJ, Fieno DS, Parrish TB, Harris K, Chen EL. Relationship of MRI delayed contrast enhancement to irreversible injury, infarct age, and contractile function. *Circulation*. 1999;100:1992-2002.
2. Weiss C, Stewart M, Franzen O, Rostock T, Becker J, Skarda JR, Meinertz T, Willems S. Transmembraneous irrigation of multipolar radiofrequency ablation catheters: induction of linear lesions encircling the pulmonary vein ostium without the risk of coagulum formation? *J Interv Card Electrophysiol*. 2004;10:199–209.
3. Schwartzman D, Ren JF, Devine WA, Callans DJ. Cardiac swelling associated with linear radiofrequency ablation in the atrium. *J Interv Card Electrophysiol*. 2001;5:159–166.
4. Wood MA, Fuller IA. Acute and chronic electrophysiologic changes surrounding radiofrequency lesions. *Journal of Cardiovasc Electrophysiol*, 2002;13:56-61.
5. Knowles BR, Caulfield D, Cooklin M, Rinaldi CA, Gill J, Bostock J, Razavi R, Schaeffter T, Rhode KS. 3-D visualization of acute RF ablation lesions using MRI for the simultaneous determination of the patterns of necrosis and edema. *IEEE Trans Biomed Eng*. 2010;57:1467–1475.
6. McGann C, Kholmovski E, Blauer J, Vijayakumar S, Haslam T, Cates J, DiBella E, Burgon N, Wilson B, Alexander A, Prastawa M, Daccarett M, Vergara G, Akoum N, Parker D, MacLeod R, Marrouche N. Dark regions of no-reflow on late gadolinium enhancement magnetic resonance imaging result in scar formation after atrial fibrillation ablation. *J Am Coll Cardio*. 2011;58:177–185.
7. Racine JS, Li Q. Nonparametric estimation of regression functions with both categorical and continuous Data. *Journal of Econometrics*. 2004;119:99–130.
8. Li Q, Racine JS. Cross-validated local linear nonparametric regression. *Statistica Sinica*. 2004;14:485–512.